Optically pumped microplasma rare gas laser

W. T. Rawlins[1,*], K. L. Galbally-Kinney[1], S. J. Davis[1], A. R. Hoskinson[2], J. A. Hopwood[2], and M. C. Heaven[3]

[1]*Physical Sciences Inc., 20 New England Business Center, Andover, MA USA 01810-1077*
[2]*Electrical and Computer Engineering Department, Tufts University, Medford, MA USA 02155-5801*
[3]*Department of Chemistry, Emory University, Atlanta, GA 30322*
* *rawlins@psicorp.com*

Abstract: The optically pumped rare-gas metastable laser is a chemically inert analogue to three-state optically pumped alkali laser systems. The concept requires efficient generation of electronically excited metastable atoms in a continuous-wave (CW) electric discharge in flowing gas mixtures near atmospheric pressure. We have observed CW optical gain and laser oscillation at 912.3 nm using a linear micro-discharge array to generate metastable Ar(4s, $1s_5$) atoms at atmospheric pressure. We observed the optical excitation of the $1s_5 \rightarrow 2p_9$ transition at 811.5 nm and the corresponding fluorescence, optical gain and laser oscillation on the $2p_{10} \leftrightarrow 1s_5$ transition at 912.3 nm, following $2p_9 \rightarrow 2p_{10}$ collisional energy transfer. A steady-state kinetics model indicates efficient collisional coupling within the Ar(4s) manifold.

OCIS Codes: (140.1340) Atomic gas lasers; (140.3380) Laser materials; (140.3460) Lasers; (140.3480) Lasers, diode-pumped

References and links

1. J. Han and M.C. Heaven, "Gain and lasing of optically pumped metastable rare gas atoms," Opt. Lett. **37**, 2157-2159 (2012).
2. J. Han, L. Glebov, G. Venus, and M.C. Heaven, "Demonstration of a diode-pumped metastable Ar laser," Opt. Lett. **38**, 5458-5461 (2013).
3. J. Han, M.C. Heaven, G.D. Hager, G.B. Venus, and L.B. Glebov, "Kinetics of an optically pumped metastable Ar laser," Proc. SPIE Paper 8962-2, LASE 2014 High Energy/Average Power Lasers and Intense Beam Applications VIII, San Francisco, CA, February (2014).
4. R.H. Page, R.J. Beach, V.K. Kanz, and W.F. Krupke, "Multimode diode-pumped gas (alkali-atom) laser," Opt. Lett. **31**, 353 (2007).
5. J.D. Readle, C.J. Wagner, J.T. Verdeyen, T.M. Spinka, D.L. Carroll, and J.G. Eden, "Excimer-pumped alkali-vapor lasers: a new class of photoassociation lasers," Proc. SPIE Paper 7581-19, LASE 2010 High Energy/Average Power Lasers and Intense Beam Applications V, San Francisco, CA, January (2010).
6. J.D. Readle, J.T. Verdeyen, J.G. Eden, S.J. Davis, K.L. Galbally-Kinney, W.T. Rawlins, and W.J. Kessler, "Cs 894.3 nm Laser Pumped by Photoassociation of Cs-Kr Pairs: Excitation of the Cs D_2 Blue and Red Satellites," Opt. Lett. **34**, 3638-3640 (2009).
7. A.V. Demyanov, I.V. Kochetov, and P.A. Mikheyev, "Kinetic study of a cw optically pumped laser with metastable rare gas atoms produced in an electric discharge," J. Phys. D: Appl. Phys. **46**, 375202 (2013).
8. Z.-B. Zhang and J. Hopwood, "Linear arrays of stable atmospheric pressure microplasmas," Appl. Phys. Lett. **95**, 161502 (2009).
9. C. Wu, A.R. Hoskinson, and J. Hopwood, "Stable linear plasma arrays at atmospheric pressure," Plasma Sources Sci. Technol. **20**, 045022 (2011).
10. N. Miura and J. Hopwood, "Spatially resolved argon microplasma diagnostics by diode laser absorption," J. Appl. Phys. **109**, 013304 (2011).
11. N. Miura and J. Hopwood, "Internal structure of 0.9 GHz microplasma," J. Appl. Phys. **109**, 113303 (2011).
12. A. Kramida, Yu. Ralchenko, J. Reader, and NIST ASD Team (2012), NIST Atomic Spectra Database (ver. 5.0), [Online]. Available: http://physics.nist.gov/asd [2013, May 13]. National Institute of Standards and Technology, Gaithersburg, MD.
13. G.P. Perram, The Air Force Institute of Technology, 2950 Hobson Way, Wright-Patterson Air Force Base, OH 45414 (personal communication, 2014).

14. X.-M. Zhu, W.-C. Chen, and Y.-K. Pu, "Gas temperature, electron density and electron temperature measurement in a microwave excited microplasma," J. Phys. D: Appl. Phys. **41**, 105212 (2008).
15. X.-M. Zhu and Y.-K. Pu, "A simple collisional-radiative model for low-temperature argon discharges with pressure ranging from 1 Pa to atmospheric pressure: kinetics of Paschen 1s and 2p levels," J. Phys. D: Appl. Phys. **43**, 015204 (2010).
16. W.T. Rawlins, K.L. Galbally-Kinney, S.J. Davis, A.R. Hoskinson, and J.A. Hopwood, "Laser excitation dynamics of argon metastables generated in atmospheric pressure flows by microwave frequency microplasma arrays," Proc. SPIE Paper 8962-2, LASE 2014 High Energy/Average Power Lasers and Intense Beam Applications VIII, San Francisco, CA, February (2014).

1. Introduction

The optically pumped rare-gas metastable laser (OPRGL) is an attractive means for efficient conversion of high-power diode laser output into gas laser output with high beam quality, at a variety of near-infrared wavelengths [1-3]. The mechanism for population inversion follows a basic three-level scheme, wherein the metastable ^3P_J rare-gas atoms (e.g. Ar(4s)), generated in an electric discharge, are optically excited to an upper state, undergo collisional energy transfer to a state at slightly lower energy to produce the inversion, and undergo lasing back to the metastable state. This scheme is analogous to the widely investigated three-level process for diode-pumped alkali lasers (DPAL) [4] and the four-level and five-level systems for exciplex-pumped alkali lasers (XPAL) [5,6]. However, the OPRGL is inherently chemically inert, and so imposes no issues with chemical hazards, high-temperature materials handling, photolytic particulate generation, and optical window degradation as experienced with DPAL systems.

The most critical aspect of investigations of the viability of OPRGL systems is the operation of a stable, continuous-wave (CW) electric discharge at atmospheric pressure (e.g., cf. [7]). Heaven and coworkers [1-3] observed the first OPRGL lasing at pressures up to 1 atm using pulsed discharges, but encountered a kinetics bottleneck to the inversion process indicating that sustained CW gain and lasing might require very high metastable concentrations produced by the discharge. Atmospheric pressure CW discharges are generally difficult to sustain, require kV-level voltages, and are typically plagued by substantial arcing and localized, short-term breakdown. We have approached the problem using linear microplasma arrays developed by Hopwood and coworkers [8,9]. These devices provide stable, spatially and temporally continuous CW operation at atmospheric pressure, at frequencies near ~900 MHz. They are compact (~25 x 35 mm circuit boards) and inexpensive, and operate at easily manageable low voltages and low powers (<30 W). The micro-discharge exhibits relatively high reduced field strength, E/N, with electron number densities in the range $10^{13\text{-}14}$ cm^{-3} and argon metastable number densities as high as 10^{13} cm^{-3} [10,11].

The relevant states of the Ar(4s, 4p) manifolds are shown in Fig. 1, with the transitions of interest highlighted. The metastable states are Ar($1s_5$, $1s_3$) (in Paschen notation); the $1s_2$ and $1s_4$ states have strong optical transitions to the ground state, however both states are radiatively trapped for our conditions. We have used a tunable, CW, 1 W titanium-sapphire (Ti:S) laser to pump the $1s_5 \rightarrow 2p_9$ transition at 811.5 nm (wavelength in air), and have observed laser-induced fluorescence, optical gain, and laser oscillation on the $2p_{10} \rightarrow 1s_5$ transition at 912.3 nm, following collisional energy transfer from $2p_9$ to $2p_{10}$.

2. Experiment description

The Ar metastables were generated by a micro-discharge array consisting of 15 micro-strip resonators, with the microplasma produced in a small gap (25 μm) between the ends of the strips and the ground plane [8,9]. Fig. 2 illustrates one side of the array circuit board. The opposite side of the board is fully covered by a ground plane. Each resonator strip is 1 mm wide, with 0.25 mm between adjacent strips. The array board was operated at a frequency near ~920 MHz, tuned to its natural resonance with the discharge off. The microplasma length along the gap was 19 mm. Based on imaging measurements of the visible and near-infrared

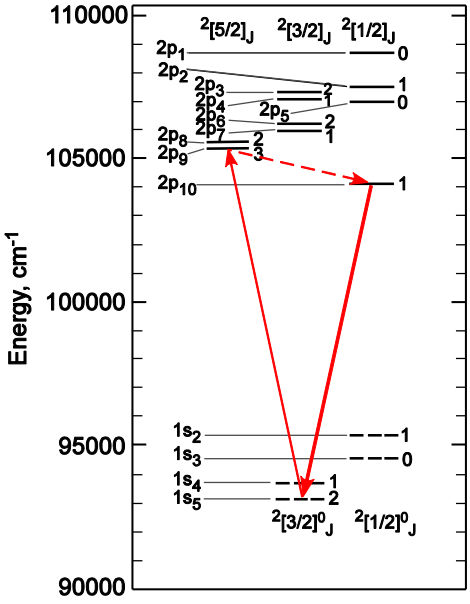

Fig. 1. Schematic illustration of Ar(I) energy levels in the 11-14 eV region: $3p^5 4s$ and $3p^5 4p$ configurations, with Paschen and Racah notation. The specific transitions observed for optical excitation, collisional energy transfer, and lasing are highlighted.

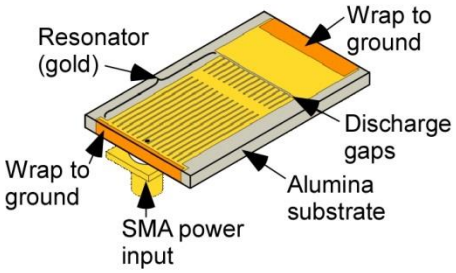

Fig. 2. Illustration of micro-discharge array board with 15 microstrip resonators. The microwave power input is the SMA connector. The micro-discharges occur in the gaps between the ends of the resonator strips and the ground.

emission, the microplasma at 1 atm extended several hundred microns both across the gap and vertically above the surface of the board. The array was housed in a discharge-flow cell which confined the gas flow in a rectangular channel along the upper surface of the board, from lower left to upper right in the figure. Approximately 2% of the gas flow passed through the active micro-discharge volume. Owing to their slow quenching in He, the discharge-produced metastables persisted downstream of the active micro-discharge for a short distance prior to entrainment and dilution into the free-stream gas flow. The discharge-flow cell consisted of a glass-filled-Teflon block with three window ports providing side and top views of the micro-discharge region, and was mounted on an x-y translation stage directly in line with the Ti:S laser beam output. Typical flow rates for these experiments were ~3.7 mmole/s (5 slm), 2% Ar in He at 1 atm. Typical net micro-discharge power was ~9 W.

A schematic of the optical system is shown in Fig. 3. The CW Ti:S pump beam and the diode laser probe beam were combined by a polarizing beamsplitter and were focused into the cell, along the line of micro-discharges produced by the 15-strip resonator array (1.9 cm path length). The transmitted beams emerging from the cell were separated by a grating and the probe beam was directed to a photodiode detector equipped with a long-pass filter to reject stray light

from the pump laser. For observations of laser-induced fluorescence (LIF) excited by the pump beam, a near-infrared (NIR) InGaAs array monochromator and InGaAs camera viewed the fluorescence through a window orthogonal to the beam axis. The camera was equipped with a 900-1100 nm bandpass filter to reject scattered light from the pump beam.

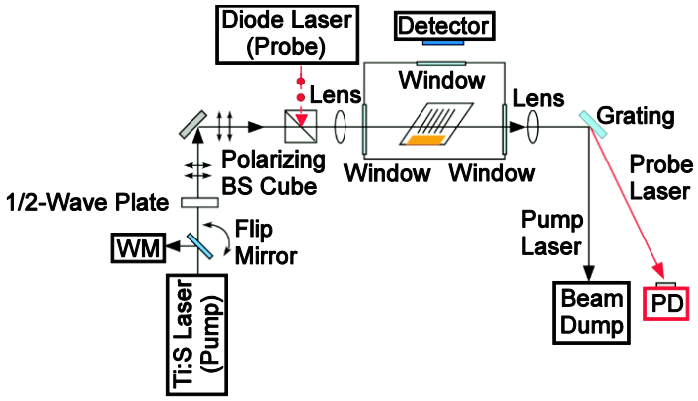

Fig. 3. Schematic of optical layout for Ar* pump/probe experiments. Direction of gas flow is out of the page. WM = wavemeter; BS = beamsplitter; PD = photodiode.

The Ti:S pump laser provided tunable CW output from 750 to ~900 nm with maximum output power up to ~0.8 W. Several choices of focusing lenses provided field-averaged pump laser intensities up to ~10 kW/cm^2 in the excitation volume. The Ti:S laser was configured as a standing wave cavity, giving line widths <2 GHz (<0.067 cm^{-1}, <4.4 pm at 811 nm). The probe laser was a fiber-coupled tunable diode laser with distributed feedback, operating near 912.3 nm with linewidth <100 MHz. The probe beam was co-aligned with the pump beam such that the probe beam diameter was always less than the pump beam diameter. The two co-aligned beams were smaller in diameter than the microplasma. The co-aligned beams were passed through the microplasma along a path just above the board surface and parallel to the line of the micro-discharge gap, 1.9 cm long. The cell position was adjusted to probe regions in, above, and downstream of the microplasma. The pump beam was tuned on and off resonance with the $1s_5 \rightarrow 2p_9$ absorption line. Incident pump beam intensity was varied by rotating the half-wave plate between the Ti:S laser and the polarizing beamsplitter (Fig. 3). By ramping the injection current, the wavelength of the probe laser was scanned repeatedly across the $1s_5 \rightarrow 2p_{10}$ line at sub-Doppler spectral resolution, measuring absorption when the pump laser was off and absorption plus gain when the pump laser was on.

3.0 Laser-induced fluorescence and optical gain

The LIF intensity at 912.3 nm, induced by the Ti:S pump laser at 811.5 nm, is proportional to the number density in the $2p_{10}$ state, and is directly related to the optical gain. A near-IR image and spatial profile of the laser-induced $2p_{10}$ fluorescence along the micro-discharge array are illustrated in Fig. 4. The camera was spectrally filtered to isolate the 900-1100 nm spectral region; the processed image was corrected for background emission from the discharge. A previously damaged resonator element is evident at ~13 mm. We observed the fluorescence with the InGaAs array monochromator to determine absolute line-of-sight column intensities near the center of the micro-discharge array. The spectrometer viewed the surface of the micro-discharge array through the top window via a fiber bundle and collimator assembly with a 1-mm aperture. The diagnostic assembly was calibrated for absolute spectral responsivity in the same configuration using a NIST-traceable blackbody source. An example spectrum of the laser-induced $2p_{10}$ fluorescence intensity, corrected for the background discharge emission, is shown in Fig. 5. The spectrum contains the Ar($2p_{10}$) emission lines at

912.30 nm ($2p_{10}\rightarrow 1s_5$) and 965.78 nm ($2p_{10}\rightarrow 1s_4$). The spectrally integrated line intensities for both the discharge-excited and LIF components show good agreement with the branching ratio given by the accepted Einstein coefficients for the transitions [12].

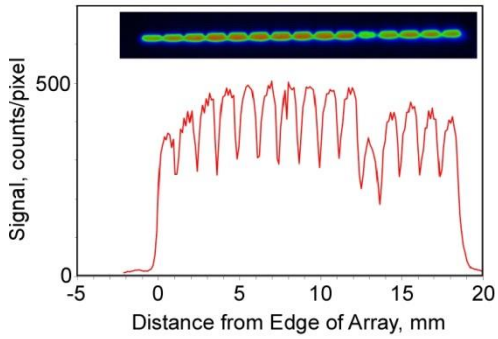

Fig. 4. Near-infrared image of the micro-discharge array (inset) and spatial profile along the array, laser-induced $2p_{10}$ fluorescence, 900-1100 nm. 6.9 kW/cm^2 Ti:S intensity at 811.5 nm, 1.0% Ar in He at 7.5 mmole/s, 767 Torr, 6.9 W net microwave power at 920 MHz. Gas flow direction in the image is from top to bottom.

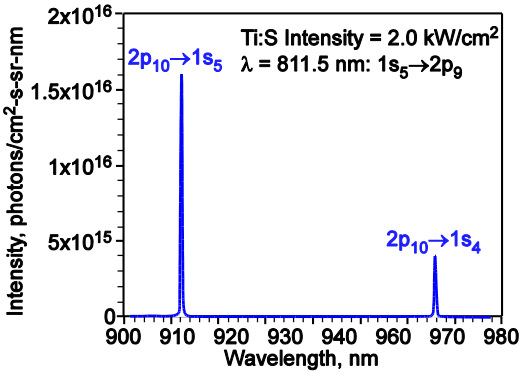

Fig. 5. Laser-induced fluorescence spectrum of the Ar $2p_{10}\rightarrow 1s_5$ (912 nm) and $2p_{10}\rightarrow 1s_4$ (966 nm) lines. 2.0 kW/cm^2 total Ti:S intensity at 811.5 nm, 4.3% Ar in He at 5.4 mmole/s, 766 Torr, 6 W net microwave power, spectral resolution 0.27 nm.

With the pump laser off and the 912 nm probe laser aligned along the 19 mm length of the micro-discharge array, we observed strong absorption upon scanning the probe laser wavelength across the $1s_5\rightarrow 2p_{10}$ line. At the nominal beam power of ~1 mW, the focused probe intensity was sufficient to slightly deplete the $1s_5$ population by optical pumping. With the probe beam intensity reduced to avoid pumping the medium, we observed $\ln(I_o/I) \sim 0.85$, corresponding to $[Ar(1s_5)] \sim 3 \times 10^{12}$ cm^{-3} produced by the discharge. The absorption line shape is consistent with pressure broadening by He at 1 atm and 600 K, assuming a representative pressure broadening coefficient of $17(T/300)^{1/2}$ MHz/Torr. This pressure broadening coefficient is consistent with recent measurements by Perram and coworkers [13].

Probe laser scans of the microplasma medium with the pump laser on and off are shown in Fig. 6. When the Ti:S pump laser was on and tuned to resonance with the $1s_5\rightarrow 2p_9$ transition at 811.5 nm, the absorption was readily inverted to a large positive gain, in this case ~0.7 cm^{-1}. The signal reverted to absorption when the pump laser was tuned off the line. Measurements of gain along the microplasma centerline for different pump laser intensities are plotted in Fig. 7. The absorption for each case was consistent throughout, verifying the stability of the microplasma during the measurement series. The small-signal gain approached saturation

(optically bleached limit) at pump laser intensities above ~2 kW/cm^2. Measurements of gain in different locations above and downstream of the micro-discharge showed considerable spatial variation, with the maximum gain near ~1 cm^{-1} located several hundred microns downstream of the active microplasma.

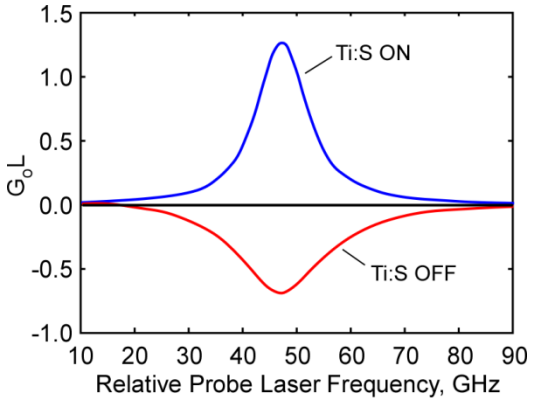

Fig. 6. Gain (Ti:S laser on) and absorbance (Ti:S laser off) on the $2p_{10}$-$1s_5$ transition at 912.3 nm, 1.9 cm path length. 2% Ar/He, 3.7 mmole/s total flow, 769 Torr, 9 W net microwave power, 4 kW/cm^2 Ti:S intensity on the $1s_5 \rightarrow 2p_9$ transition at 811.5 nm.

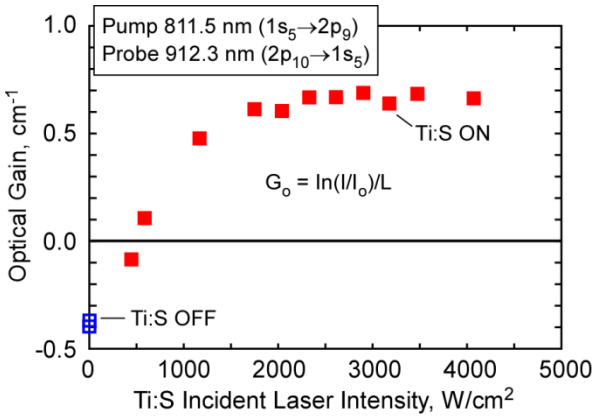

Fig. 7. Optical gain along the microplasma centerline versus incident pump intensity. 2% Ar/He at 3.7 mmole/s, 769 Torr, 9 W net microwave power.

4.0 Laser power extraction

To demonstrate laser power extraction, we assembled a hemispherical stable resonator for longitudinal pumping, using a mirror separation which supports the TEM_{00} mode with a mode diameter less than the diameter of the focused pump laser beam. To achieve this configuration, we modified the optical setup for gain measurements shown in Fig. 3. We removed the two lenses on either side of the flow cell, focused the pump laser beam with a 250 mm focal length lens placed between the turning mirror and the polarizing beamsplitter, placed a high-reflectivity (>99.9%) mirror at a right angle to the beamsplitter (in place of the probe laser in Fig. 3), and installed an output coupling mirror in place of the lens on the beam-exit side of the flow cell. Light transmitted by the output mirror was dispersed by the grating and 912 nm light was directed to a photodiode equipped with a 912 nm narrow bandpass

filter. Top-view images of the $2p_{10}$ LIF by the NIR camera verified the alignment of the pump beam, microplasma, and laser cavity. The 250 mm lens gave a nearly constant pump beam waist of ~250 μm diameter along the length of the micro-discharge array.

Immediately prior to the first lasing experiments, we measured the small-signal gain in the optimum-gain location slightly downstream of the active micro-discharge. For this measurement, the high-reflectivity mirror was replaced by the probe laser and by a 150 mm focal length lens to focus the probe beam inside the pump beam, and the output mirror was removed. The emerging probe beam was directed onto the photodiode via the grating. The total Ti:S pump power was 800 mW, corresponding to 1320 W/cm^2 along the length of the micro-discharge array. The discharge-flow conditions were 2% Ar in He at 3.7 mmole/s total flow rate, 770 Torr, 9 W net microwave power. The single-pass gain in this configuration was $G_oL = 2.2$, or $G_o = 1.1$ cm^{-1}. This signifies a single-pass amplification of exp(2.2) = 9, i.e. nearly an order of magnitude on each pass through the cavity.

For the same discharge-flow and optical pumping conditions, using the hemispherical optical resonator and two mirrors with reflectivities greater than 99.9% at 912 nm, we readily obtained stable laser oscillation. With the photodiode positioned to observe the light passing through the output coupler, the observed signal level was 24 nA at 912 nm when the Ti:S pump laser was tuned into resonance with the $1s_5 \rightarrow 2p_9$ transition at 811.5 nm, 0.75 nA when the pump laser was tuned off resonance, and 0.05 nA when the pump laser beam was blocked. The contrast between on-resonance and off-resonance readings confirmed that the signal was due to the optically pumped $2p_{10} \rightarrow 1s_5$ transition.

We observed two beam reflections off the grating, one corresponding to the 811 nm pump beam and one corresponding to 912 nm. With the photodiode positioned to observe the 912 nm spot on the grating, adjustment of the cavity alignment via the two mirrors increased the photodiode signal to 400 nA. This sensitivity to cavity alignment confirmed that the emission was due to coherent lasing and not incoherent amplified spontaneous emission (ASE).

Next we replaced the output coupler mirror on the cavity with a mirror that had ~15% transmission at 912 nm. In this configuration we measured 22 mW output power at 912 nm, and the pump power absorbed by the medium was ~40 mW. Thus, the apparent optical-to-optical conversion efficiency was ~55%. The optically pumped laser ran continuously and stably for at least 30 minutes, until we shut off the pump laser.

We imaged the laser spot on the grating with the near-IR camera, and the result is shown in Fig. 8. The 912 nm spot was well separated spatially from the 811 nm pump laser spot. The image in Fig. 8 is corrected for the background image obtained with the pump laser tuned off resonance. The beam profile is Gaussian indicating a high quality beam, with no evidence of distortion by the flow field or the microplasma medium.

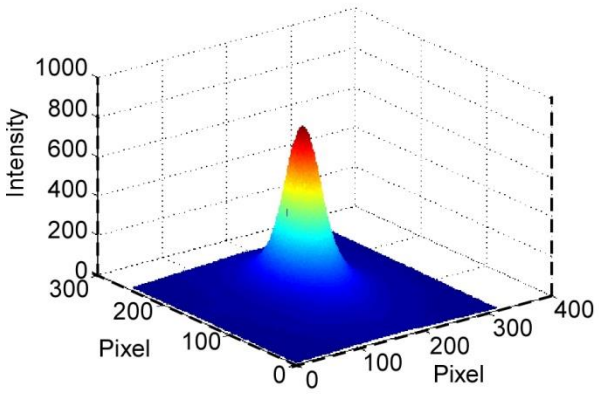

Fig. 8. 3-D image of optically pumped argon metastable laser output beam at 912.3 nm.

5.0 Discussion

The experimental results provide an empirical metric for the relationship between the open-loop gain and the unpumped, discharge-produced Ar($1s_5$) number density, [Ar*], for the saturated (bleached) limit at high pump intensities: $[Ar^*]/G_o = (4\pm1)\ x10^{12}\ cm^{-2}$ at 1 atm, 2% Ar/He mixtures, and 9 W discharge power. It is straightforward to show through a steady-state kinetics analysis that G_o is directly proportional to [Ar*] in the saturated regime, and that the $[Ar^*]/G_o$ ratio decreases with increasingly efficient spin-orbit coupling kinetics.

The kinetics model must include the role of the $1s_4$ state populated by radiative decay from the $2p_{10} \rightarrow 1s_4$ branch of the $2p_{10}$ fluorescence. This transition, at 966 nm, accounts for 21.3% of the radiative decay rate of the $2p_{10}$ state; the $2p_{10} \rightarrow 1s_3$ and $2p_{10} \rightarrow 1s_2$ transitions at 1047 and 1149 nm are much less significant, comprising 3.84% and 0.75% of the total, respectively [12]. Han et al. [2,3] observed slow collisional energy transfer from $1s_4$ to $1s_5$, with a rate coefficient for He on the order of $10^{-13}\ cm^3/s$ at room temperature, resulting in a significant bottleneck in the replenishment of $1s_5$ population. Those results raised significant questions about the viability of this system for continuous-wave lasing, while the present results demonstrate the opposite.

To examine this point, we consider the steady-state model for the four-state system illustrated in Fig. 9. The figure denotes excitation and deactivation rates, where levels 1, 2, 3 and 4 represent the Ar $1s_5$, $2p_{10}$, $2p_9$, and $1s_4$ states respectively. In this scheme, level 1 is optically excited to level 3, which is collisionally coupled to level 2, creating a population inversion between levels 2 and 1. I is the excitation laser intensity transmitted by the medium, B_{13} and B_{31} are the Einstein absorption and stimulated emission coefficients for 1↔3, A_{31} is the Einstein spontaneous emission coefficient for 3→1, k_c is the rate coefficient for collisional energy transfer from 3 to 2, *[M]* is the number density of the bath gas (in our case, He at 1 atm and 600 K), A_{21} is the Einstein spontaneous emission coefficient for 2→1, k_Q is the rate coefficient for quenching of 2→1, B_{12} and B_{21} are the absorption and stimulated emission coefficients for 1↔2, and I' is the transmitted intensity of stimulated emission from 2 to 1. To incorporate the fourth state, we add A_{24}, the Einstein coefficient for 2→4 emission, k_{41}, the rate coefficient for collisional energy transfer from $1s_4$ to $1s_5$, and k_{14}, the reverse rate coefficient determined by detailed balance. (The energy of the $1s_4$ state of Ar is 606.83 cm^{-1} above that of $1s_5$ [12], ~1.5kT at the nominal discharge temperature ~600 K.) The strongly allowed resonance transition (A_{40}) from $1s_4$ to the ground state (106.6 nm) is optically thick over a dimension of a few microns for our experimental conditions, and thus the $1s_4$ state population is radiatively trapped. Han et al. [2,3] observed an effective radiative loss rate of (4 to 6) x $10^5\ s^{-1}$ for this state, which is small compared to the collisional coupling terms. If the optical pumping process is confined to only these four states, then the total number density of all four is equivalent to the initial $1s_5$ metastable number density in the absence of optical excitation ([Ar*]).

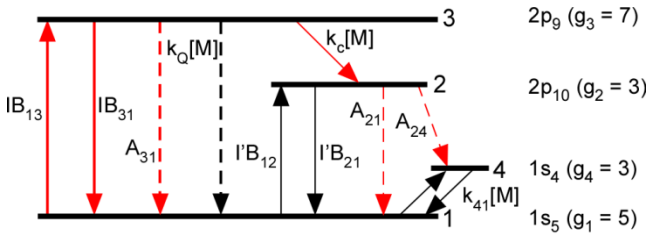

Fig. 9. Illustration of four-level model with excitation and deactivation terms.

For the case of open-loop gain (no mirrors or lasing), the 1↔2 stimulated emission terms can be neglected. The resulting steady-state solution is a transcendental set of six equations

for the populations of each state, the total population of all four states, and the transmitted pump beam intensity:

$$n_3 = \frac{IB_{13}}{IB_{31} + A_{31} + \left(k_c + k_Q\right)[M]}\, n_1 \tag{1}$$

$$n_2 = \frac{k_c[M]}{A_{21} + A_{24}}\, n_3 \tag{2}$$

$$n_1 = \frac{\left(IB_{31} + A_{31} + k_Q[M]\right) n_3 + A_{21} n_2 + k_{41}[M]\, n_4}{IB_{13} + k_{14}[M]} \tag{3}$$

$$n_4 = \frac{A_{24} n_2 + k_{14}[M]\, n_1}{k_{41}[M] + A_{40}} \tag{4}$$

$$n_{TOT} = n_1 + n_2 + n_3 + n_4 \tag{5}$$

$$I = \frac{I_0}{\delta\nu} \int_O^L \exp\left(-\sigma_{13} N_{13} z\right) dz, \;\; N_{13} = n_1 - \frac{5}{7} n_3 \tag{6}$$

The spontaneous (A_{ij}) and stimulated (B_{ij}) emission Einstein coefficients are taken from data available in the NIST atomic spectroscopy data base [12]. We have incorporated the room-temperature collisional energy transfer rate coefficients for M = He as reported by Han et al. [2,3] for $2p_9$-$2p_{10}$ and $1s_4$-$1s_5$ collisional coupling. For present purposes, we focus on the solution for the saturated (optically bleached) limit, where the pump intensity *I* is so large that the stimulated emission terms IB_{31} and IB_{13} overwhelm the spontaneous emission and collisional deactivation rates for n_1 and n_3. In this limit, we have $n_3/n_1 = B_{13}/B_{31} = g_3/g_1 = 7/5$, the medium is essentially transparent to the pump beam, and the state populations and optical gain are independent of pump intensity. The gain is then determined by a straightforward algebraic solution in terms of [Ar*]: $[Ar^*]/G_o = 1.53 \times 10^{13}$ cm^{-2}. The relative state populations approach constant values: $n_3/n_1 = 1.4$, $n_2/n_1 = 12.1$, and $n_4/n_1 = 31.9$. Thus the $1s_4$ state (n_4) takes up 69% of the total population when the 4-state ensemble is optically pumped. Our gain data show that this is clearly not the case for the conditions of our micro-discharge flow experiments.

If the collisional coupling between $1s_4$ and $1s_5$ is fast, e.g. the populations of the two states are in thermal equilibrium, we can neglect the $1s_4$ state and reduce the set of equations to a three-state model. The steady-state model provides analytical solutions of the state populations and gain as functions of incident pump intensity and total metastable concentration. Example results are shown in Fig. 10, small-signal gain versus pump intensity for two different initial $1s_5$ number densities, 5×10^{12} and 1×10^{13} cm^{-3}. The steady-state model predicts an exponential increase in both the laser-induced fluorescence and the gain to a saturated level, as observed experimentally. The differences between the predicted and observed saturation intensities require further investigation. In the saturated or optically bleached limit, the scaling of gain with total initial $1s_5$ number density is $[Ar^*]/G_o = 5.69 \times 10^{12}$ cm^{-2}, in reasonable agreement with the experimental result. Thus it appears that the population of the $1s_4$ state remains small in our CW discharge conditions, in contrast to the observations of Han et al. [2,3] for pulsed discharges near 300 K.

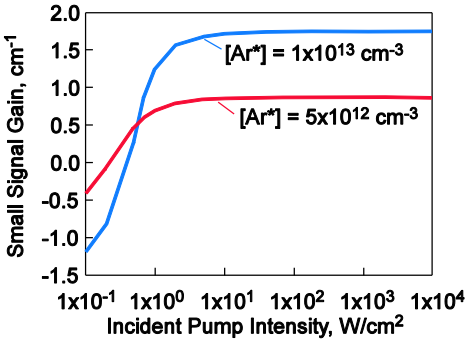

Fig. 10. Steady-state three-level model predictions of Ar($2p_{10}$→$1s_5$) optical gain as a function of incident excitation laser intensity, for two different initial Ar($1s_5$) number densities.

We can eliminate electron collisions as significant contributors to this picture. For the likely electron densities and typical excitation and superelastic quenching rate coefficients [14,15], the first-order rates for electron quenching from $1s_4$ to $1s_5$ are smaller than the neutral-atom collisional coupling rates at 1 atm. Furthermore, we observe gain downstream of the active micro-discharge, where the local electron density is greatly depleted.

We consider instead the effect of the elevated temperature in the discharge-flow system, ~600 K. If we assume an idealized Arrhenius temperature scaling of the rate coefficient, $k = Ae^{-B/T}$, where A ~ 3 x 10^{-10} cm^3/s (nominal gas-kinetic limit), the room-temperature measurements of Han et al. [2,3] suggest a maximum value B ~ 2300 K. Then the value of k_{41} would scale to 6.5 x 10^{-12} cm^3/s at 600 K, and that of k_{14} would increase accordingly by detailed balance. This leads to $[Ar^*]/G_o$ = 5.1 x 10^{12} cm^{-2}, in much better agreement with the experimental results and essentially the same as that obtained by the three-state model. Indeed, the discrepancy can be resolved with an even weaker temperature dependence: a $1s_4/1s_5$ population ratio as much as 10 times the 600 K thermal ratio gives reasonable agreement with the gain data [16]. Application of similar Arrhenius scaling to the $2p_9 \rightarrow 2p_{10}$ collisional energy transfer rate coefficient k_c yields excellent agreement with the data: k_c(600 K) ~ 7.2 x 10^{-11} cm^3/s, $[Ar^*]/G_o$ = 4.3 x 10^{12} cm^{-2}.

The results of this model-data comparison exercise suggest a possible pathway for scaling rare-gas metastable lasers to higher gain through moderate heating of the gas flow. Gas temperatures are typically several hundred K in CW micro-discharges [10,11], and may increase as a result of simple scaling of micro-discharge volume and microwave power, as well as pump laser power deposition. To more firmly establish this idea, we need accurate rate coefficient measurements at elevated temperatures, more detailed optically pumped gain measurements for a variety of discharge-flow conditions, and systematic direct sampling of the individual state number densities. The present results confirm the validity of the optically pumped rare-gas laser for CW operation, as well as the coupling of optical pumping with atmospheric-pressure microplasmas as a means of producing laser oscillation.

Acknowledgments

We thank Prof. Glen P. Perram (Air Force Institute of Technology), and Dr. Gordon D. Hager (Albuquerque, NM) for helpful technical discussions and generous data exchanges. Mr. David C. Rossi and Dr. Seonkyung Lee (Physical Sciences Inc.) assisted with the apparatus design and assembly. This work was supported by the High Energy Laser Joint Technology Office through a Multidisciplinary Research Initiative with Emory University (FA9550-13-1-0002), by the Air Force Research Laboratory/AFMC (FA8650-12-C-2312, Dr. Steve Adams, COTR), by the Air Force Office of Scientific Research, and by Physical Sciences Inc. internal funds.